Lone-Pair-Induced Covalency as the Cause of Temperature- and Field-Induced Instabilities in Bismuth Sodium Titanate

Denis Schütz, Marco Deluca, Werner Krauss, Antonio Feteira, Tim Jackson, and Klaus Reichmann*

Bismuth sodium titanate (BNT)-derived materials have seen a flurry of research interest in recent years because of the existence of extended strain under applied electric fields, surpassing that of lead zirconate titanate (PZT), the most commonly used piezoelectric. The underlying physical and chemical mechanisms responsible for such extraordinary strain levels in BNT are still poorly understood, as is the nature of the successive phase transitions. A comprehensive explanation is proposed here, combining the short-range chemical and structural sensitivity of in situ Raman spectroscopy (under an applied electric field and temperature) with macroscopic electrical measurements. The results presented clarify the causes for the extended strain, as well as the peculiar temperature-dependent properties encountered in this system. The underlying cause is determined to be mediated by the complex-like bonding of the octahedra at the center of the perovskite: a loss of hybridization of the $6s^2$ bismuth lone pair interacting with the oxygen p-orbitals occurs, which triggers both the field-induced phase transition and the loss of macroscopic ferroelectric order at the depolarization temperature.

1. Introduction

Contemporary high-precision micropositioning systems and sensors rely on the outstanding electromechanical properties exhibited by lead zirconate titanate (PZT)-based solid solutions. The ability to control the electromechanical performance of PZT via chemical doping is certainly one of its most attractive features. Hence, PZT can be employed either in the fabrication of actuators (such as fuel-injection valves or micropositioning systems) or in sensors (such as pressure and acceleration sensors). Indeed, PZT owes its tremendous commercial success to this unique versatility. Nevertheless, from a health perspective, the manipulation of toxic lead oxide during the fabrication of PZT-based components and their later disposal partially overshadows its technological merits. A ban of lead in electronic components is expected to be enforced as soon as some alternative materials are made available. Obviously, this poses restrictions on the further applicability of PZT and motivates the search for valid lead-free alternatives that are capable of reproducing its behavior at least partly. However, the substitution of PZT by lead-free materials has emerged to be more challenging than expected. Possible candidates are potassium sodium niobate (KNN) solid solutions for "hard"[1] applications where low losses and high coupling factors are necessary and bismuth sodium titanate (BNT) solid solutions for "soft" applications, like actuators, where the ability to extend under an applied electric field is of paramount importance. This latter material has been the focus of a plethora of structure- and application-related studies recently. Although initially characterized in the 1960s,[2] BNT solid solutions have seen a revival of research interest in recent years[3] due to the discovery of extended strains under high fields that surpass those reached by PZT.[4,5] This property makes BNT an excellent candidate for the replacement of PZT in actuators, despite its piezoelectric coefficient (d_{33}) being considerably lower than that of PZT under low field intensities.[6] The mechanism of the extended strain and especially its structural and chemical origins is, however, poorly understood. In addition, the high field intensities necessary to drive this effect still constitute a technological obstacle that needs to be overcome.

The crystal structure of BNT and its solid solutions has been extensively studied. At room temperature, all binary solid solutions replacing the univalent A-site cation (with the notable exception of Li substitution[6]) exhibit a phase transition from rhombohedral ($R3c$) (in recent studies, monoclinic Cc[8]) to

D. Schütz, Dr. W. Krauss, Prof. K. Reichmann
Christian Doppler Laboratory for Advanced Ferroic Oxides
Institute for Chemistry and Technology of Materials
Graz University of Technology
Stremayrgasse 9/3, A-8010 Graz, Austria
E-mail: denis.schuetz@tugraz.at
Dr. M. Deluca
Institut für Struktur- und Funktionskeramik
Montanuniversitaet Leoben
Peter Tunner Straße 5, A-8700 Leoben, Austria
Dr. M. Deluca
Materials Center Leoben Forschung GmbH
Roseggerstraße 12, A-8700 Leoben, Austria
Dr. A. Feteira
Christian Doppler Laboratory for Advanced Ferroic Oxides
School of Chemistry
University of Birmingham
Edgbaston, B15 2TT, Birmingham, UK
Dr. T. Jackson
School of Electronic, Electrical and Computer Engineering
University of Birmingham
Edgbaston, B15 2TT, Birmingham, UK

DOI: 10.1002/adfm.201102758

tetragonal (*P4bm*)[3], forming a morphotropic phase boundary (MPB) in between. In contrast to PZT, this MPB is not temperature invariant but is bent over a wide temperature range, leading to strong temperature dependences of the desired properties. This has been confirmed by high-resolution techniques,[7,8] utilizing both X-ray[9] and neutron scattering.[10] However, due to the inclusive nature of any bulk-scattering technique, this description should be considered only as the average long-range symmetry of the material.[10] Transmission-electron-microscopy (TEM) measurements of the material have indicated a stronger unstable nature of BNT with respect to PZT: different researchers have found different symmetries for the same nominal compositions,[11] both within the same sample,[8,12] and even within the same grain.[13] In other words, there is evidence that the room-temperature phase is, in fact, composed of three different symmetries (*Pm-3m*, *P4bm*, and *R3c*)[11,14] that coexist without macroscopic separation and that they are very close to each other with regard to the crystallographic cell constants, but not in symmetry.[11,14,15] These aspects have also been confirmed by means of Raman spectroscopy, both in pure BNT[16,17] and its solid solutions.[18–20] Room-temperature phase coexistence provides an explanation for the sensitivity of the material to processing parameters, or even to sample preparation before measurement.[11]

Another feature shared by all BNT solid solutions exhibiting an extended strain is the existence of an intermediate temperature-triggered phase transformation (in the range <100–250 °C, depending on the substituents) from the dominantly ferroelectric (FE) room-temperature phase to a (pseudo)-cubic phase. As increasing temperature above this point is accompanied by a loss of macroscopic ferroelectricity; this transition temperature is unanimously referred to as the depolarization temperature (T_d). The phase above T_d has been described as either anti-ferroelectric (AFE)[4] or nonpolar[21] (a term that includes anti-ferroelectric phases by definition) and is still subject to considerable debate in the literature. Its existence is, however, undisputed and can be easily verified from ε–T measurements, being visible as anomalies in both the relative permittivity and the loss factor (**Figure 1**). T_d can be shifted by the introduction of a low molar concentration of dopants, producing a downward (most prominently with Nd and Nb[6,22]) or upward shift (e.g., Fe). In this regard, two application-related approaches can be found in the literature. While some groups try to increase T_d and operate within the FE regime,[6] the other approach is to lower the T_d and operate within the nonpolar (AFE) regime, a safe distance from any phase transition, thus exploiting the field-driven extended strain. This latter choice is extremely advantageous for technological applications, since (together with avoiding the bent MPB) it allows the strain of the BNT solid solutions to be made temperature-independent within defined conditions.[23,24]

At the upper border of the nonpolar phase, the material presents relaxor ferroelectric behavior, which is signaled by the lack of a clear Curie–Weiss peak in ε–T measurements[25] and the frequency dispersion.[26] This is generally associated with the presence of polar nanoregions (directly observed at elevated temperatures[21]), which are credited to be the basis of such diffuse behaviour,[27] although other explanations are also being discussed.[28] The region of the diffuse *T*-dependent phase transition in relaxors where ergodic polar nanoregions fluctuate is

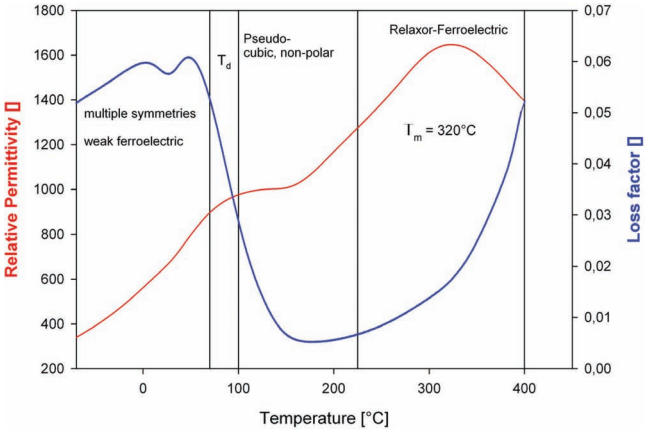

Figure 1. Temperature dependence of the relative permittivity and loss factor of BNT-BKT at 1 kHz. The temperature range in which the peculiar electromechanical behavior appears is indicated. T_d occurs at 70–100 °C, whereas the permittivity maximum in the region of the fluctuating nanoregions is assigned as T_m.

sometimes called the Burns region,[26] and the peak where they percolate is known as the Burns temperature (T_m).[25] This is physically different to the Curie temperature (T_C), which marks a sharp transition to a paraelectric phase.[29] The relaxor behavior is thought to be the result of the large lattice size and a valence mismatch at one of the cation sites, leading to the disorder-driven nucleation of polar nanoregions at high temperature and a subsequent frequency dispersion. In the most studied relaxor material, lead magnesium niobate (PMN), this criterion is satisfied by the B-site (Mg:Nb), whereas in BNT-solid solutions, it is fulfilled by the A-site (Bi:Na, Bi:K). Subsequent disorder phenomena stem from this occurrence.[25] Recently, evidence has been found that the covalent bond present in perovskites with A-site cations possessing lone pairs can cause additional disorder if the site occupancy is significantly less than 100%,[30–32] causing a superposition of short-range behavior on the long-range behavior.

The field-dependent behavior of BNT-derived materials is as peculiar as their temperature-dependent behavior. Interestingly, strain curves for materials exhibiting extended strain under a field show no occurrence of remnant strain[4,5,22,27] under a cyclic electric load (i.e., no characteristic "butterfly" hysteresis curves are found). Unlike the strain reported in conventional ferroelectric materials, the curve is not constantly linear, but can always be separated into: i) a low-strain part at low field (d_{33} < 100 pm V^{-1}); ii) an electrostrictive part exhibiting second-order curvature at intermediate fields; and iii) a ferroelectric part at high field showing a linear (first-order) curve[3,24,33] (cf. **Figure 2**).

Likewise, the polarization curves show a characteristic pinched loop under a cyclic electric field (similar to anti-ferroelectric materials) with little or no remnant polarization.

Comparing these datasets with the strain curves (Figure 2), the pinched region coincides with the low-strain part, the region from the opening, to the onset of saturation with the electrostrictive part, and the region of saturation, with the linear part, suggesting at least one additional phase transition under field.

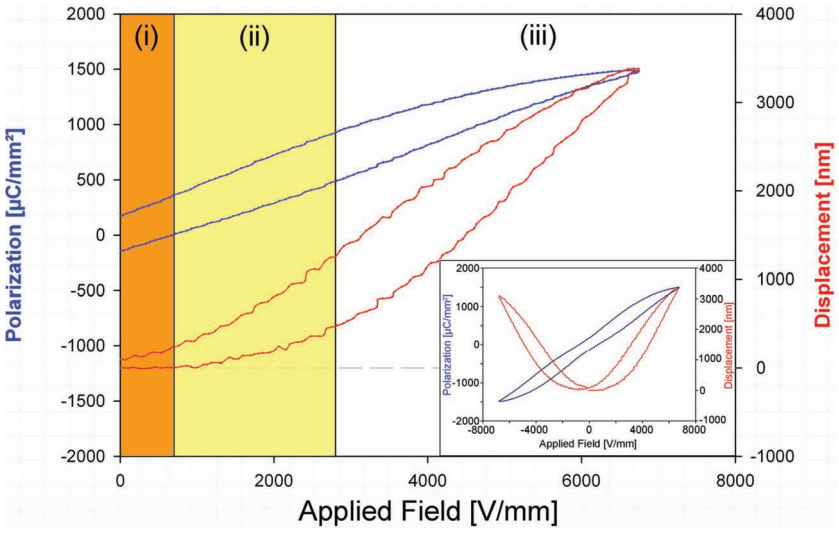

Figure 2. The positive part of the polarization- and strain versus applied electric field loops for BNT-BKT. The complete curves are shown in the inset. The regions indicated in the diagram are responsible for the peculiar electromechanical behavior and are related to a particular structure of the material: i) low-strain region, weak ferroelectric; ii) electrostrictive region, nonpolar (AFE); and iii) ferroelectric linear region, presence of polar nanodomains.

The structural mechanisms at the basis of this behavior are not clear, and in order to elucidate them, in situ field-dependent measurements capable of detecting symmetry changes or the development of ferroelectric ordering are necessary.

Daniels et al.[34] found a phase transition from pseudocubic to tetragonal above 3 kV mm^{-1}, confirming one phase transition under field. However, due to the initial field strength being too high, the first suggested phase transition from zero-field ferroelectric to nonpolar (AFE), which typically occurs from 0.5–1 kV mm^{-1}, would not have been visible in this experimental setup. The field intensity, however, coincides with the transition from nonpolar (electrostrictive) to ferroelectric relaxor (the beginning of the linear strain curve (Figure 2) behavior.

Similar results were reported in a recent study by Simons et al.[14] for a nominally rhombohedral composition. Again, the initial applied field was too large to expose any potential structural change occurring between the low strain and the electrostrictive regimes. Field-dependent TEM experiments performed by Kling et al.[11,35] showed a ferroelectric ordering (domains) developing under applied electric field, but, correspondingly, they were unable to reveal a possible phase transition under low fields.

The main open questions on BNT-based materials thus involve the field-dependent phase transitions (especially at low fields) and the structural mechanisms of transitions, measured in dependence of both the electric field and the temperature.

Recently, we manufactured a prototype stack featuring 50 active, 35 μm-sized layers of a neodymium-doped BNT-BKT (bismuth potassium titanate) ceramic,[23] which exhibits less than 10% variation of strain between 20 °C and 150 °C. In eschewing the MPB region of the BNT-BKT material in favor of more-temperature-stable properties, we chose to exploit the high-field-driven strain of the AFE phase. Nd was thus added to depress the T_d, and Li to improve the sintering characteristics. The low thickness of the active layers allowed the stack to be handled safely under the needed high fields. Applying 200 V to the stack resulted, in fact, in a field intensity of 7 kV mm^{-1}, more than enough to trigger field-dependent effects, unlike in bulk samples (usually 1 mm in thickness), which would need 7000 V of applied electric tension to reach the same field intensities.

In this work, we combine strain and polarization measurements under high electric fields with in situ temperature- and field-dependent micro-Raman spectroscopic investigations of BNT-BKT stacks. The aim of our study was to clarify the nature of the above-mentioned phase transitions under temperature and field changes, supporting our reasoning with the results of the chemical- and structure-sensitive Raman technique.

Raman spectroscopy has already been used to detect phase changes in BNT-based solid solutions in dependence of temperature[9,16,18–20] and pressure.[36] Due to the intrinsic static disorder of BNT, and to the splitting of simultaneously Raman and IR-active bands into longitudinal-optical (LO) and transverse optical (TO) components, the Raman spectrum of BNT appears very broad; thus, a thorough assignment of the Raman modes is challenging. Consequently, detection of symmetry changes in dependence of temperature has seldom been reported.[17] This notwithstanding, previous Raman studies have confirmed the presence of the diffuse phase transition at T_d and linked it with the presence of polar nanodomains.[20,37] In this work, we build upon these findings, and provide, for the first time, a comprehensive study of BNT-BKT in dependence of both temperature and applied field. Special attention is given here to the A-site modes, since their behavior gives insight to the chemical peculiarities of the A–O bonds. Raman spectroscopy allows us to detect changes occurring at the short-range; the small interaction volume of this technique has the further advantage that, unlike in scattering experiments, the (Ag/Pd) electrode layer does not influence the measurements, making the stack-shaped samples ideal for this combined temperature- and field-dependent in situ approach.

2. Results

2.1. Electromechanical Behavior of BNT-BKT

The multilayer-stack object of our study was a modified BNT-BKT solid solution, with a low molar concentration of dopants introduced to improve performance. This composition shows all of the typical hallmarks of this class of materials, including a T_d, a relaxor transition and extended strain under high fields. The displacement and polarization curves show characteristics common to all solid solutions of BNT exhibiting extended strain. The only difference is a shift of T_d to lower values due to

Nd addition.[6] Consequently, this composition can be taken as a typical example, and the phase transition phenomena highlighted here can be applied to any non-MPB composition.

The temperature-dependent electrical measurements are summarized in Figure 1. We assigned the T_d, signified by the sudden drop in loss factor and relative permittivity, to be within the region between 70 °C and 100 °C. The beginning of the region of fluctuating nanoregions was found to be at approximately 220 °C, extending to 400 °C with a peak, the Burns temperature being 320 °C. The uncertainties of the heating-stage arrangement, as well as the diffuse nature of both phase transitions[3,11,26] make a more-accurate assignment difficult.

The electromechanical measurements of the stack can be seen in Figure 2. By visual inspection according to Rödel et al.[24,33] the first transition point was found to be at ≈0.7 kV mm^{-1}, signifying a transition from the low-strain regime to electrostrictive characteristics, whereas the transition to linear strain coinciding with the nonpolar to FE phase transition was assigned at ≈2.8 kV mm^{-1}.

2.2. The Raman Spectrum of BNT-BKT

The room-temperature crystal structure of the end members of the BNT-BKT solid solution has been reported as being rhombohedral *R3c* for BNT and tetragonal *P4bm* for BKT.[9] For compositions in the neighborhood of the MPB, generally a mixture of both phases has been reported.[11] Factor-group analysis leads to 13 simultaneously IR and Raman active modes for the *R3c* structure[16]: $\Gamma_{R3c,\ \mathrm{Raman}} = 4A_1 + 9E$. For the tetragonal *P4bm* structure of BKT, a total of 16 Raman-active modes are predicted, of which only 12 (of A_1 and E symmetry) are simultaneously infrared active[9,16]: $\Gamma_{P4bm,\ \mathrm{Raman}} = 4A_1 + 1B_1 + 3B_2 + 8E$. The Raman modes of A1 symmetry are associated with lattice displacements parallel to the *c*-axis of the unit cell, whereas the twofold-degenerate E modes represent phonons propagating perpendicular to the *c*-axis.[38] The simultaneous IR and Raman activity produces additional splitting of each A1 and E mode into their longitudinal-optical (LO) and transverse-optical (TO) components, so that, in principle, up to 24 and 28 modes should be visible for the *R3c* and *P4bm* unit cells, respectively. However, the scattering efficiency of some of these modes may be weak,[9] and, generally in BNT-based materials, they contribute (together with the additional Raman activity caused by short-range disorder[20]) only by increasing the width of neighboring modes with a higher intensity. Similar considerations apply in the case of a monoclinic *Cc* structure.[38] For the above reasons, all of the Raman modes in BNT-based materials are convoluted into three main observable peaks, and a complete assignment of the underlying phonon modes has never been reported.

Depolarized Raman spectra of (Li, Nd)-doped BNT-BKT in dependence of temperature and applied electric field are displayed in **Figure 3**a and 3b, respectively. The spectra have been corrected for the Bose–Einstein population factor. Spectral deconvolution was performed according to 13 Gaussian–Lorentzian peak functions by means of a best-fitting algorithm. The spectrum is consistent with previous reports,[9] and can be linked to a mixed rhombohedral-tetragonal crystal structure. The three main regions can be distinguished in the spectrum;

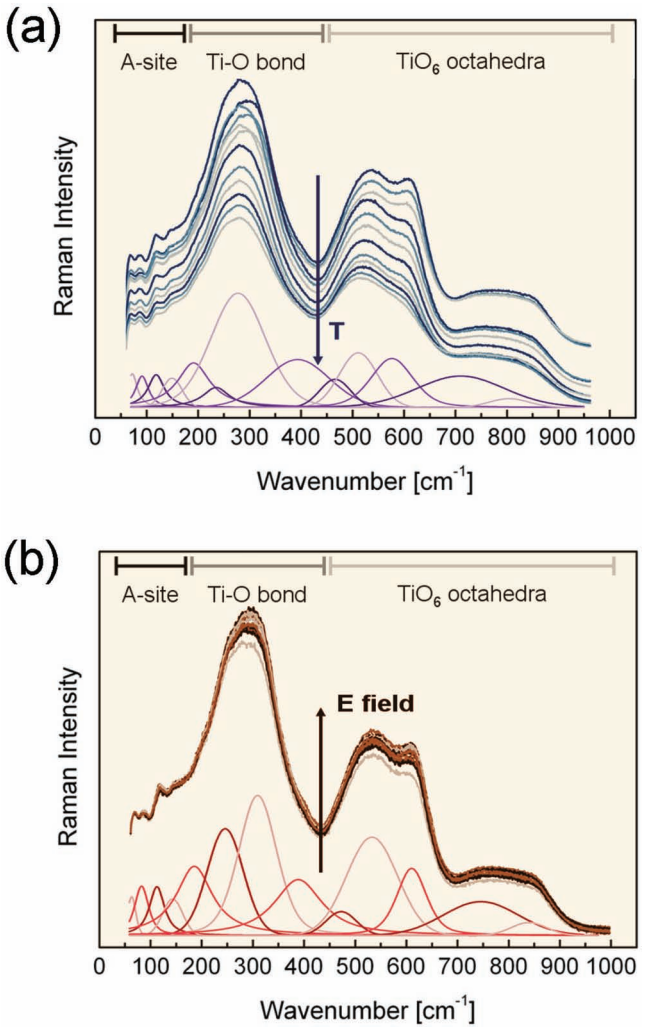

Figure 3. a,b) Depolarized Raman spectrum of Li/Nd-doped BNT-BKT as a function of temperature (a) and applied electric field (b). The spectra were deconvoluted according to 13 Gaussian–Lorentzian peak functions, and the fitting is displayed for high values of both temperature and field. The assignment of the spectral modes to particular lattice vibrations is also indicated.

each of them has a relationship with different kinds of vibration in the lattice:

- Wavenumbers < ≈150 cm^{-1}: these modes can be associated with vibrations of the perovskite A-site, thus involving Bi, Na, K and Li cations. The presence of such distinct modes in this frequency range suggests possible cation ordering at the A-site. In order to provide sufficient Raman scattering to result in an observable mode, the size of the ordered clusters must, in fact, encompass at least ≈20 unit cells.[9] The mode at ≈135 cm^{-1} has previously been assigned as belonging to A_1 symmetry[39] and, more recently, associated with Na–O/K–O vibrations.[9] By means of considerations purely referring to the cation mass on the A-site, we can thus assign the two modes at ≈145 cm^{-1} and ≈115 cm^{-1} to Na–O/K–O vibrations, and the other modes to vibrations involving the Bi–O bond (85 cm^{-1} and 65 cm^{-1}).[9,40] The Li content was very low, so supposedly should not give rise to a visible peak.

- Wavenumber range 150–450 cm^{-1}: modes in this region can be associated with Ti–O vibrations. Especially, the mode with the highest intensity, at 305 cm^{-1}, has been assigned as an A_1 mode closely related to the strength of the Ti–O bond.[9] Soft-mode behavior in dependence of temperature has been reported previously for this peak.[18]
- The high-frequency bands above 450 cm^{-1} have all been associated with TiO_6 vibrations, namely the breathing and stretching modes of the oxygen octahedra. In the range 450–700 cm^{-1} (i.e., the second "hump" in the spectrum), three modes are observed, which have been previously assigned as A_1(TO) (at 485 cm^{-1}), A_1(LO) (at 540 cm^{-1}) and overlapping E(LO) and E(TO) modes (at 620 cm^{-1}).[9,36] However, the angular dependence of the intensity of the mode at 620 cm^{-1}, together with the temperature-dependent behavior similar to the mode at 305 cm^{-1}, suggest that this mode belongs to A_1 symmetry.[18,41] The broad, higher-frequency bands (the third "hump") are understood to be an A_1(LO) and E(LO) overlap.[9,18]

The fitting reported in Figure 3a,b refers to high values of temperature and applied field, respectively. For increasing temperature, the spectrum undergoes broadening and some of the modes (the ones at ≈245 cm^{-1} and ≈620 cm^{-1}, for instance) decrease their intensity. This is associated with the material becoming more BNT-like. In other words, there is a loss of polarity of the unit cell – the material resembles the pseudocubic structure. On the other hand, for high values of applied field (Figure 3b), the splitting of the Ti–O modes is preserved, and the material becomes more BKT-like. This signifies an increase in the polar character of the unit cell (i.e., more tetragonality).

2.3. Interpretation of Temperature Effects

The temperature dependence of the position, intensity and full width at half maximum (FWHM) of both the A-site-related and B-site-related modes are shown in **Figure 4**. In the absence of any phase transition, one would expect a steady phonon softening and an increase in mode FWHM with temperature. However, in the case of BNT-BKT, two clear anomalies are visible at ≈100 °C and ≈225 °C.

The first anomaly is an abrupt change in the phonon wavenumber (softening of the phonon modes) that takes place in the A-site-related modes at 100 °C. We caution the reader that the mode at ≈65 cm^{-1}, being located close to the cut-off of the filter, should be considered only for qualitative comparisons. Nevertheless, changes in this mode are reflected in all neighboring A-site modes, which demonstrates the reliability of our fitting procedure.

For higher temperatures, the modes steadily harden, up to ≈225 °C, above which they become nearly temperature-independent. This anomaly is also reflected in a change in the FWHM of the Ti–O and octahedra-related modes (cf. Figure 4f); namely, above 100 °C the FWHM values of the modes at ≈305 cm^{-1}, ≈485 cm^{-1} and ≈620 cm^{-1} increase. The softening of the A-site modes is due to a weakening of the bonding between the A-site cations and oxygen. Considering the presence of a lone-pair in Bi^{3+}, we suggest that this anomaly is related to the loss of orbital hybridization between the $6s^2$ orbitals of the Bi^{3+} and the oxygen p orbitals. Hybridization of the A-site lone pairs with oxygen was postulated as early as the 1950,[25,42–44] and is credited as being the reason for the high Curie temperature of lead titanate and PZT.[43] This high T_C cannot be explained otherwise, and the effect is called either covalency[45] or the "lone-pair effect"[46] in the literature. Warren et al.[47] credited the hybridization of the lead $6s^2$ orbitals with oxygen, together with the resulting displacement, as the deciding factors for the enhanced ferroelectric properties of lead (zirconium) titanate.

Mechanistically speaking, this occurrence is possible through the hybridization of orbitals in the octahedral $[Ti(Zr)O_6]^{2-}$ structure found at the center of most perovskite ferroelectrics.[48,49] The empty d-shell of the central atom leads to a hybridization and shift in electron density from oxygen towards Ti^{4+}, a process that has been described to be very similar or identical to d^0 transition-metal-ligand systems found in complex chemistry.[49,50] This, in turn, depletes the bonded oxygen atoms of electron density in the direction of the A-site, allowing the lone pair ($6s^2$) of Bi^{3+} to hybridize with the oxygen's depleted p-orbitals, allowing a metal-oxygen-metal (B-O-A site, respectively) bond to form, thus distorting the octahedron.[50] This point can be illustrated by the contour plots of electron density found within Zhurova and Tsirelson's[51] treatment of $SrTiO_3$, and, even more clearly, in the theoretical treatments of BNT by Zeng et al.[52] and Gröting et al.,[53] who stated that "the strong hybridization effects of Ti–O and Bi–O states are obvious".

The "lone-pair effect" is also evident in the case of doping barium titanate with Pb^{2+}, Bi^{3+} or Tl^{+}[45] cations, which share a common electronic structure ([Xe] $4f^{14}5d^{10}6s^2$) in their preferred oxidation states, thus exhibit lone pairs and, together with the octahedral $[Ti(Zr)O_6]^{2-}$ structure, a lone-pair effect.[54]

Structurally, perovskites without a lone-pair-carrying A-site behave reliably according to Goldschmidt's tolerance factor,[55] their symmetry being exclusively governed by their ionic radii. Goldschmidt discovered a relationship between the ionic radii of A- and B-site cations in perovskites and their long-range crystal structure (Equation 1):

$$\tau = \frac{R_A - R_0}{\sqrt{2}(R_B + R_0)} \quad (1)$$

where τ is the Goldschmidt (or tolerance) factor, and R_A, R_B and R_O denote the Shannon radii of the A, B and oxygen sites, respectively.

A crystal system with a Goldschmidt factor above 1 means that the material is unable to form a non-hexagonal perovskite due to the A-site cations being too large to fit within the interstitial sites. A tolerance factor above 0.9 signifies an ideal cubic perovskite, while factors from 0.9 to 0.71 force rhombohedral, tetragonal or even monoclinic symmetries, at which point Glazer's octahedral tilt system[9,15] comes into play.

Materials with a lone-pair effect, like PZT, do not behave this way because their structure is constrained by the additional factor of A-site lone pairs bonding with the electron-depleted side of the oxygen, instead of the 12 nearly equidistant ionic bonds that are encountered in perovskites like barium titanate, whose A-site ions carry no lone pair.

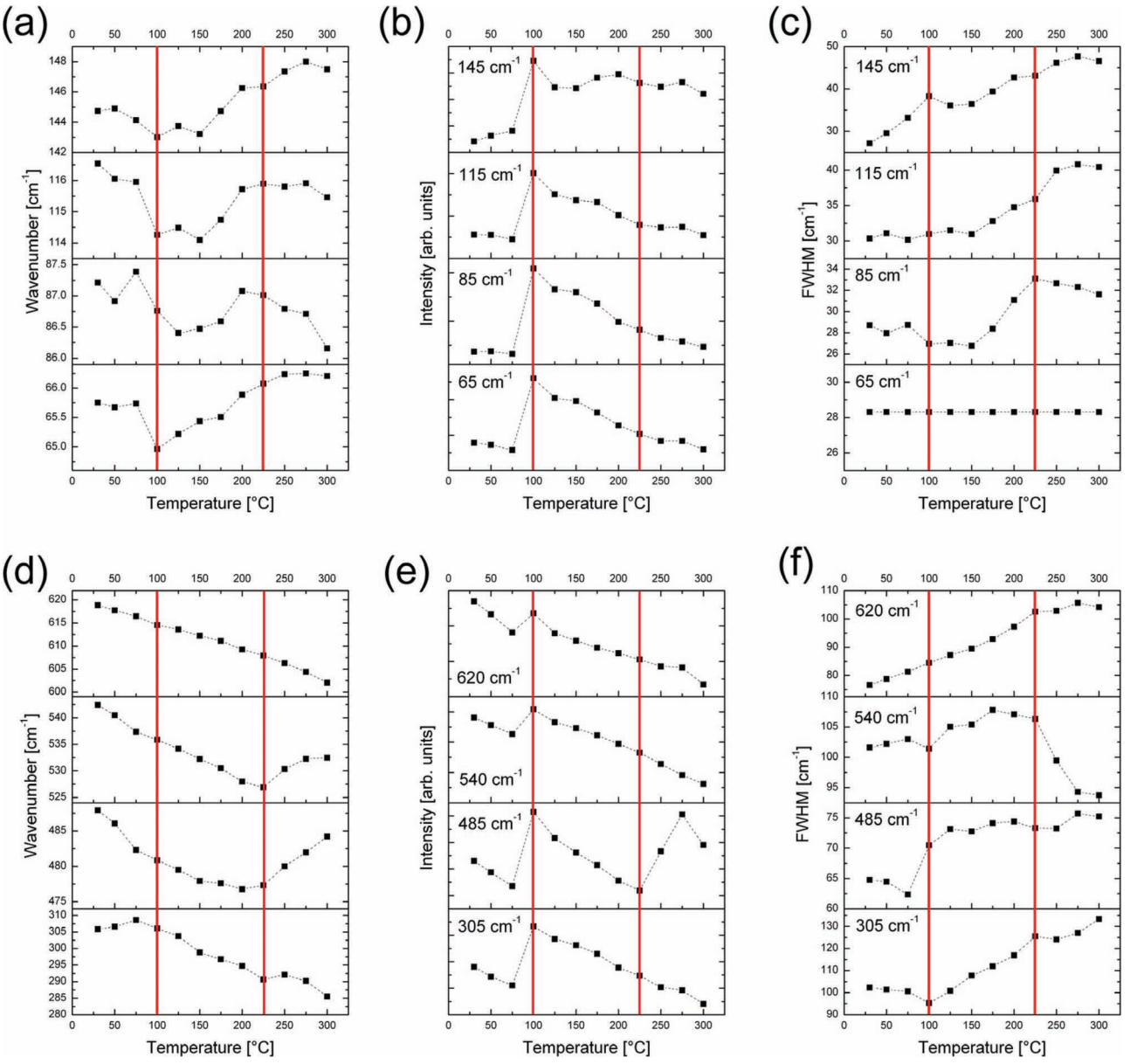

Figure 4. Temperature dependence of selected modes of the BNT-BKT spectrum. a–c) The peak position, intensity and FWHM of the A-site-related modes, respectively. d–f) The peak position, intensity and FWHM for the B-site modes. The FWHM of the 65 cm^{-1} mode was kept fixed during fitting. The dashed lines connecting the experimental points are merely guides to the eye. The locations of the anomaly points (100 °C and 225 °C) are indicated by the red vertical lines.

All BNT solid solutions of research interest have a tolerance factor between 0.98 and 1, putting them firmly within the range of an ideal cubic perovskite.[56] However, at room temperature, they show average long-range symmetries from tetragonal to rhombohedral, reaching a (pseudo-)cubic state at T_d. This type of distortion of the underlying octahedra has been documented in numerous non-perovskite oxides (as well as in PZT and its end members) with an octahedrally co-ordinated d^0 transition metal at the center of the complex.[50] The resulting distortion from a lone-pair-carrying atom at either: the edge (C_2), point (C_4) or face (C_3) of the octahedra, would produce tetragonal (C_4), rhombohedral (C_3) or orthorhombic (C_2) distortions, respectively, in a perovskite lattice. This hybridization has been shown to be breakable by thermal vibration (see report by Halasyamani[50] and references therein). Also, Ti^{4+} in combination with Bi^{3+} has been noted to have a clear preference for the (C_4) distortion.

From the Raman results and the aforementioned theory, one can conclude that the mechanism at T_d is neither displacive nor order-disorder, but is rather mediated by the loss of hybridization of Bi^{3+} and oxygen through thermal vibrations along the polar axis. The sudden drop in the wavenumber of the A-site

modes at the transition point, T_d, can, in fact, be interpreted as a weakening of the A–O bonds. The consequent hardening of the modes can be then associated with the influence of the residual electrostatic forces at play between the Bi-ion lone pair and the oxygen atoms. This exact mechanism happens in PZT as well, but, due to the uniform A-site occupancy, coincides with the Curie temperature.

As a result of this change in the bond situation, a higher polarizability of the unit cells, resulting in the possible formation of nanodomains, is conceivable. This seems indeed in accordance with the behavior of the mode FWHM above 100 °C for the A-site, B-site and octahedral modes. In fact, we observed an increase in mode FWHM (cf. Figure 4c and 4f), signifying a higher degree of disorder in the lattice. Apart from the possible presence of nanodomains, this result confirms that the transition at 100 °C changed the symmetry of the complete unit cell from its constrained room-temperature state to the (pseudo-) cubic state (with tetragonal nanodomains in the case of this composition) predicted by the ionic radii. This is strong evidence that the mechanism of the depolarization phase transition is in fact mediated by the loss of constraint put upon the crystal system through the lone-pair effect of the Bi–O bond facilitated by thermal vibration. It is usually sufficient to postulate a change in bonding within a molecule if a change in the interatomic spring constant (A-site modes, specifically Bi–O modes) is accompanied by a change in symmetry of the whole molecule. Both criteria were satisfied with regard to the T_d. Additionally, the changes visible by Raman spectroscopy were corroborated by macroscopic *T*-dependent electrical measurements.

Why the Bi–O bond is more fragile than the Pb–O bond in PZT (where the polar phase is stabilized) is unknown; most likely, it is related to the site occupancy of the bismuth, which is usually at or less than 50% of an A-site. In addition, steric effects from the other members of the shared A-site would also have an influence. The shared site occupancy of bismuth, taken in connection with the fragile Bi–O bond and the random nature of the site occupancy[53,,57] between bismuth and the univalent counterion, can also serve to explain the fragile nature of the room-temperature state, where a mixture of competing symmetries is found.[11] The bent MPB can, in turn, be described by a combination of the steric effects of larger or smaller univalent A" ions being incorporated into the lattice. The Bi–O bonds, being weakened by the increased thermal vibrations, will, in fact, lose their constraining effect upon a temperature gradient, thus easing mixed A-site substitution and eventually producing the bent MPB. The straight MPB of PZT is, in turn, produced by the homogeneous A-site occupancy of lead[29,43,50] without compositional steric effects.

The second anomaly at 225 °C is related to the transition to the region of fluctuating nanoregions, as proven by the temperature dependence of the B-site and the octahedral modes. The Ti–O mode at ≈305 cm^{-1} (Figure 4d) initially undergoes softening, which demonstrates a smooth decrease of the unit-cell anisotropy with increasing temperature. The smooth shrinkage of the unit cell is then interrupted at 225 °C. The same temperature marks an anomaly in both octahedra-related modes, at 485 and 540 cm^{-1}: both modes harden for $T > 225$ °C. These two modes likely belong to E symmetry, whereas the mode at 620 cm^{-1}, showing a similar behavior (Figure 4d) to the one at 305 cm^{-1}, is confirmed to possess A_1 symmetry. These considerations suggest that the ongoing structural change occurs mainly in one crystallographic direction. Since the Ti–O bonds and the octahedral vibrations are influenced by the dynamics of the nanodomain phase,[58] this behavior is compatible with a diffuse phase transition marking the beginning of the region of fluctuating nanoregions (Figure 1), in which the material presents a macroscopic relaxor behavior. This was also confirmed by the ε–*T* measurements. In a word, the Raman spectroscopy results confirm that, with increasing temperature, a more disordered lattice is obtained, and this is mediated by a weakening of the Bi–O hybrid orbitals, which promotes an enhanced polarizability of the unit cell.

2.4. Influence of an Applied Field

The electric-field dependence of the Raman spectra of BNT-BKT is reported in **Figure 5**: the peak position, intensity and FWHM of the A-site modes are shown in Figure 5a–c, respectively. Figure 5d–f illustrate the same for the B-site modes. Two main anomalies, seen as an increase in the wavenumber of the Bi–O related peaks, are visible for increasing applied field, at ≈0.7 kV mm^{-1} and at ≈2.8 kV mm^{-1}. In addition, a sharpening of the octahedra-related mode at ≈620 cm^{-1} occurs in the low-field regime. Please note that this mode underwent broadening upon increasing temperature (Figure 4f). Regarding the B-site modes, it is noticeable that, during the whole range of applied field, the Ti–O mode at ≈305 cm^{-1} hardens constantly. This is the same mode that showed a steady softening with the anomaly at ≈225 °C, in the temperature dependence. The effect of the applied field is thus the opposite of that of temperature: applied field reduces disorder in the lattice (i.e., sharpening of modes) and increases the polarity of the unit cell (i.e., mode hardening and the spectrum resembling the BKT material). This appears to be mediated by a change occurring on the A-site at ≈0.7 kV, which is reflected in the oxygen octahedra as well (i.e., an anomaly in the A-site- and B-site-mode positions). This could be similar to the supposed loss of hybridization that occurs at 100 °C, with the only difference being that, by increasing the temperature, a more-disordered lattice was obtained due to the presence of nanodomains produced by bond weakening (i.e., a more-cubic lattice), while these nanodomains will orient themselves under increasing field into the field direction and thus produce a more-polar (i.e., more-tetragonal) lattice. This can indeed be connected to the field-induced giant strain that is observed in this material. In other words, the low-strain regime of the material (0–0.7 kV mm^{-1}) is governed by the small intrinsic converse piezoelectric effect, whereas the electrostrictive regime (0.7–2.8 kV mm^{-1}) can be linked to the metastable state introduced through the weakening of the Bi–O bond. This gives rise to a more-cubic regime, whereas the final linear part could be related to the nucleation of tetragonal (in other compositions rhombohedral), polar nanodomains within the (pseudo)-cubic matrix. This aspect can be pointed out considering the anomalies in the peak positions of the A-site and B-site modes at ≈2.8 kV mm^{-1} and, especially, the mode FWHM increase for the Ti–O peak (at ≈305 cm^{-1}) above 2.8 kV mm^{-1} (i.e., higher disorder in the

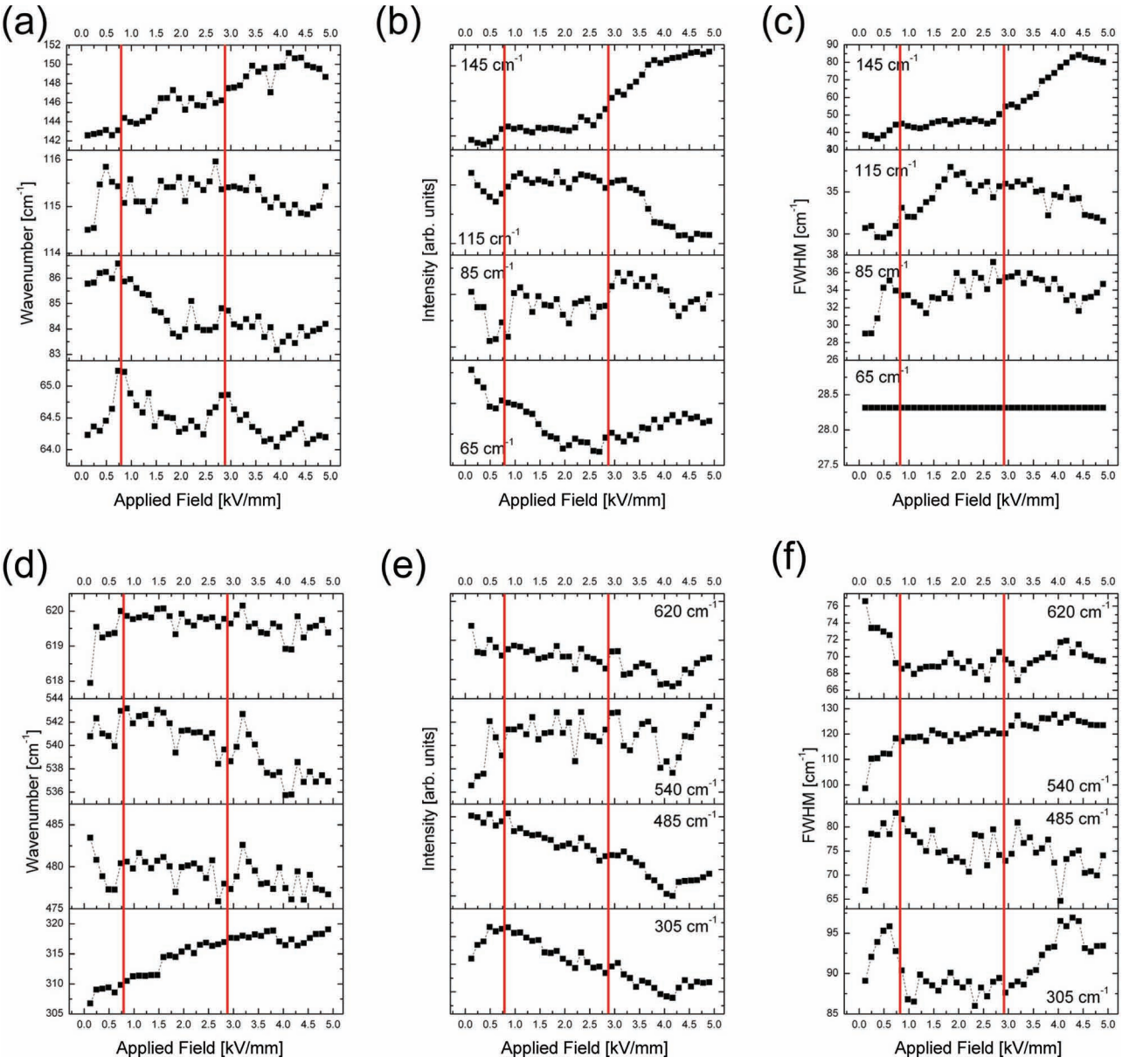

Figure 5. Electric-field dependence of selected modes of the BNT-BKT spectrum. a–c) The peak position, intensity and FWHM of the A-site-related modes. d–f) The peak position, intensity and FWHM of the B-site modes. The FWHM of the 65 cm^{-1} mode was kept fixed during fitting. The dashed lines connecting the experimental points are merely guides to the eye. The locations of the anomaly points (0.7 kV mm^{-1} and 2.8 kVmm^{-1}) are indicated by the red vertical lines.

lattice above this point). Conveniently, electrostrictive effects tend to be more pronounced in perovskites with a structure close to cubic (PMN etc.),[59,60] thus explaining the behavior of the material during the electrostrictive part of the strain curve. Consequently, if this is the cause for the extended strain, any electromechanical measurement of the material above or approaching T_d should show an immediate electrostrictive curve from low fields as well as a more pinched polarization loop. This exact behavior is widely seen within different solid solutions of BNT[23,24,54,61] (and also within our stack), confirming this aspect of our analysis. The gradual transition into ferroelectric relaxor behavior is, in essence, a field-forced nonpolar (AFE)-to-ferroelectric phase transition, which has been documented in numerous anti-ferroelectrics.[62] This is the phase transition observed by Daniels[34] and Simons[14] in their in situ scattering experiments under a field. The behavior, especially in the electrostrictive regime and above, can therefore be understood as a metastable state with multiple states accessible with a minimal change in intrinsic energy → a flat free-energy surface (see report by Damjanovic[63] and references therein). Unlike conventional ferroelectrics, this region is not compositional, but field- and temperature-dependent, and occurs through a wide compositional range. In summary, the field-dependency results, in correlation with the temperature-dependency results,

show that the phase transition at higher fields and the gradual loss of Bi–O covalence are, in fact, interrelated. These findings are in accordance with previously published in situ data[64] and also with recent modeling work on this system.[53] In addition, a recent paper using the same experimental method has shown polar nanoregions developing in Bi^{3+}-doped $KNbO_3$ as a consequence of the lone pairs interacting with the oxygen octahedra,[65] which further strengthens our conclusions.

3. Conclusions

We have shown that the depolarization temperature is a result of the breaking of Bi–O hybridization and the subsequent release of the constraint it puts upon the crystal system. This allows the structure to reset itself to the symmetry dictated by its ionic radii. This observation is linked to the potential instability of the room-temperature state of this type of ceramic material, as well as the bent nature of the MPB. As expected, the relaxor ferroelectric nature of the material above the nonpolar AFE phase region was substantiated and an order/disorder-driven effect based upon the A-site was confirmed. This also confirms previous field-dependent measurements. Thus, the mechanism of the extended-field-induced strain in BNT solid solutions is a succession of different effects that are linked by a common cause. The Bi–O bond breaking leads to the introduction of a more cubic regime (or a mixture of nanodomains in a pseudocubic matrix) favoring the electrostrictive response in the second regime. The subsequent field-induced nonpolar (AFE)-to-FE phase transition under high field is also a direct consequence of this symmetry change and the applied field, accounting for the linear part of the electromechanical curve at high fields. There is still a lot to be understood about the system, especially regarding the role of vacancies, processing routes and their influence on the switching behavior, as well as the exact nature of the phase above T_d, but a further step in understanding this complex system has been taken.

4. Experimental Section

The ceramic powder for the multilayer-stack had a composition of $[Bi_{0.49}Nd_{0.01}Na_{0.335}K_{0.125}Li_{0.04}]TiO_3$, and was made by a modified mixed oxide process. The reagent-grade raw materials were Bi_2O_3 (HEK-Oxides), Na_2CO_3 (Merck), K_2CO_3 (Merck), Li_2CO_3 (Merck), TiO_2 (Tronox) and Nd_2O_3 (Treibacher). The raw materials were ball-milled for 5 h in a laboratory ball-mill (Dyna–Mill Multi Lab) with water as a solvent, and were subsequently dried using a laboratory spray-dryer. After calcination at 900 °C for 2 h, additionally 1 mol% of Nd_2O_3 was added and a second milling for 5 h and drying took place with the same equipment. From this powder, a water-based slurry was made with a binder, and tape casting was performed on laboratory equipment. 50 layers were printed with Ag/Pd-metal paste (70/30), stacked in a format of 10 × 10 cm, with additional covering layers, and they were pressed under a uniaxial load of 100 tons. After dicing and binder burnout, sintering took place in air at a temperature of 1100 °C for 5 h. The final dimensions were 7 × 7 × 2 mm with an active-layer thickness of approximately 35 µm. The sintered multilayer stacks were contacted with silver paste (burn-in temperature: 750 °C) for the electric measurements. Before any measurement, the stack was poled at 7 kV mm^{-1}.

Depolarized Raman spectra were obtained in back-scattering geometry using a micro-Raman spectrometer (Model InVia, Renishaw, New Mills, UK), equipped with a Rayleigh line-rejection edge filter that was set for the 532 nm excitation of an Ar^+ ion laser, which allowed ripple-free measurements down to 50 cm^{-1} from the laser line. Spectra were acquired using a 50× microscope objective and a laser power of 10 mW focused on a spot of ≈ 2 µm. The Raman spectra were obtained at 20 K intervals in the temperature range 300 –570 K using a temperature stage (THM600 Linkam, Tadworth, UK). The electrical-field-dependent spectra were acquired at 2 V intervals up to 200 V, using a high-voltage power supply.

The temperature dependence of the permittivity was measured using a Novocontrol Concept 40 impedance analyzer. Measurements were performed from –100 °C to 400 °C at a heating rate of 2 K min^{-1}. The polarization and displacement curves were measured using an aixPES Piezoelectric Evaluation System from aixACCT, from room temperature to 150 °C.

Acknowledgements

This work was supported by EPCOS OHG, a group company of the TDK-EPC Corporation, especially by Michael Schossmann, who attended to the processing of the multilayer sample with great care and commitment. Funding was provided by the Christian Doppler Research Association, Austria. M.D. gratefully acknowledges financial support by the Austrian Federal Government (in particular from the Bundesministerium für Verkehr, Innovation und Technologie and the Bundesministerium für Wirtschaft und Arbeit) and the Styrian Provincial Government, represented by Österreichische Forschungsförderungsgesellschaft mbH and by Steirische Wirtschaftsförderungsgesellschaft mbH, within the research activities of the K2 Competence Centre on "Integrated Research in Materials, Processing and Product Engineering", operated by the Materials Center Leoben Forschung GmbH in the framework of the Austrian COMET Competence Centre Programme. Dr. Jens Kreisel (INP Grenoble, France) is gratefully acknowledged for discussions on the interpretation of the Raman spectroscopy results in the BNT-based materials.

Received: November 15, 2011
Published online: March 13, 2012

[1] S. Zhang, J. B. Lim, H. J. Lee, T. R. Shrout, *IEEE Trans. Ultrason., Ferroelect. Freq. Control* **2009**, *56*, 1523.
[2] G. Smolenskii, V. Isupov, A. Agranivyskaya, N. Krainik, *Sov. Phys. –Solid State IV* **1960**, *2*, 2651.
[3] J. Rödel, W. Jo, K. T. P. Seifert, E.-M. Anton, T. Granzow, *J. Am. Ceram. Soc.* **2009**, *92*, 1153.
[4] S.-T. Zhang, A. B. Kounga, E. Aulbach, T. Granzow, W. Jo, H.-J. Kleebe, J. Rödel, *J. Appl. Phys.* **2008**, *103*, 034107.
[5] S.-T. Zhang, A. B. Kounga, E. Aulbach, W. Jo, T. Granzow, H. Ehrenberg, J. Rödel, *J. Appl. Phys.* **2008**, *103*, 034108.
[6] T. Takenaka, H. Nagata, *J. Eur. Ceram. Soc.* **2005**, *25*, 2693.
[7] E. Aksel, J. S. Forrester, J. L. Jones, P. A. Thomas, K. Page, M. R. Suchomel, *Appl. Phys. Lett.* **2011**, *98*, 152901.
[8] C. Ma, X. Tan, E. Dul'kin, M. Roth, *J. Appl. Phys.* **2010**, *108*, 104105.
[9] J. Kreisel, A. M. Glazer, G. Jones, P. A. Thomas, L. Abello, G. Lucazeau, *J. Phys.: Condens. Matter* **2000**, *12*, 3267.
[10] S. Gorfman, P. A. Thomas, *J. Appl. Crystallogr.43*, **2010**, 1409.
[11] L. A. Schmitt, J. Kling, M. Hinterstein, M. Hoelzel, W. Jo, H.-J. Kleebe, H. Fuess, *J. Mater. Sci.* **2011**, *46*, 4368.
[12] X. Tan, E. Aulbach, W. Jo, T. Granzow, J. Kling, M. Marsilius, H.-J. Kleebe, J. Rödel, *J. Appl. Phys.* **2009**, *106*, 044107.
[13] L. A. Schmitt, H.-J. Kleebe, *Funct. Mater. Lett.* **2010**, *03*, 55.
[14] H. Simons, J. Daniels, W. Jo, R. Dittmer, A. Studer, M. Avdeev, J. Rödel, M. Hoffman, *Appl. Phys. Lett.* **2011**, *98*, 082901.

[15] M. Troccaz, P. Gonnard, Y. Fetiveau, L. Eyraud, G. Grange, *Ferroelectrics* **1976**, *14*, 679.
[16] J. Petzelt, S. Kamba, J. Fábry, D. Noujni, V. Porokhonskyy, A. Pashkin, I. Franke, K. Roleder, J. Suchanicz, R. Klein, G. E. Kugel, *J. Phys.: Condens. Matter* **2004**, *16*, 2719.
[17] L. Luo, W. Ge, J. Li, D. Viehland, C. Farley, R. Bodnar, Q. Zhang, H. Luo, *J. Appl. Phys.* **2011**, *109*, 113507.
[18] D. Rout, K. S. Moon, V. S. Rao, S. J. L. Kang, *J. Ceram. Soc. Jpn.* **2009**, *117*, 797.
[19] D. Rout, K. S. Moon, S. J. L. Kang, I. W. Kim, *J. Appl. Phys.* **2010**, *108*, 084102.
[20] B. Wylie-van Eerd, D. Damjanovic, N. Klein, N. Setter, J. Trodahl, **2010**, *Phys. Rev. B: Condens. Matter 82*, 104112.
[21] C. W. Tai, S. H. Choy, H. L. W. Chan, *J. Am. Ceram. Soc.* **2008**, *91*, 3335.
[22] Z. Shujun, T. R. Shrout, H. Nagata, Y. Hiruma, T. Takenaka, *IEEE Trans. Ultrason. Ferroelect. Freq. Control* **2007**, *54*, 910.
[23] W. Krauss, D. Schütz, M. Naderer, D. Orosel, K. Reichmann, *J. Eur. Ceram. Soc.* **2011**, *31*, 1857.
[24] K. T. P. Seifert, W. Jo, J. Rödel, *J. Am. Ceram. Soc.* **2010**, *1396*, 1392.
[25] R. E. Newnham, *Properties of Materials: Anisotropy, Symmetry, Structure*, Vol. *1*, Oxford University Press, Oxford **2005**.
[26] A. A. Bokov, Z. G. Ye, *J. Mater. Sci.* **2007**, *1*, 31.
[27] T. R. Shrout, S. J. Zhang, *J. Electroceramics* **2007**, *19*, 113.
[28] R. Blinc, *J. Phys. Chem. Solids* **2000**, *61*, 177.
[29] B. Jaffe, W. R. Cook, H. L. C. Jaffe, *Piezoelectric Ceramics*, Academic Press, London **1971**.
[30] A. Feteira, D. C. Sinclair, J. Kreisel, *J. Am. Ceram. Soc.* **2010**, *93*, 4174.
[31] V. Shuvaeva, D. Zekria, A. M. Glazer, Q. Jiang, S. M. Weber, P. Bhattacharya, P. A. Thomas, *Phys. Rev. B: Condens. Matter* **2005**, *71*, 174114.
[32] W. Dmowski, S. B. Vakhrushev, I.-K. Jeong, M. P. Hehlen, F. Trouw, T. Egami, *Phys. Rev. Lett.* **2008**, *100*, 137602.
[33] W. Jo, T. Granzow, E. Aulbach, J. Rödel, *J. Appl. Phys.* **2009**, *105*, 094102.
[34] J. E. Daniels, W. Jo, J. Rödel, J. L. Jones, *Appl. Phys. Lett.* **2009**, *95*, 032904.
[35] J. Kling, X. Tan, W. Jo, H.-J. Kleebe, H. Fuess, J. Rödel, *J. Am. Ceram. Soc.* **2010**, *93*, 2452.
[36] J. Kreisel, A. M. Glazer, P. Bouvier, G. Lucazeau, *Phys. Rev. B: Condens. Matter* **2001**, *63*, 1.
[37] E. Aksel, J. Forrester, B. Kowalski, M. Deluca, D. Damjanovic, J. L. Jones, *Phys. Rev. B: Condens. Matter* **2012**, *B 85*, 024121.
[38] R. Loudon, *Adv. Phys.* **1964**, *13*, 423.
[39] M. S. Zhang, J. F. Scott, J. A. Zvirgzds, *Ferroelect. Lett. Section* **1986**, *6*, 147.
[40] V. N. Denisov, A. N. Ivlev, A. S. Lipin, B. N. Mavrin, V. G. Orlov, *J. Phys.: Condens. Matter* **1997**, *9*, 4967.
[41] I. Gregora, P. Ondrejkovic, E. Simon, M. Berta, M. Savinov, J. Hlinka, H. Luo, Q. Zhang, *Ferroelectrics* **2010**, *404*, 220.
[42] J. B. Goodenough, *Phys. Rev.* **1955**, *100*, 564.
[43] G. Shirane, R. Pepinsky, B. C. Frazer, *Acta Crystallogr.* **1956**, *9*, 131.
[44] A. Villesuzanne, C. Elissalde, M. Pouchard, J. Ravez, *Eur. Phys. J. B* **1998**, *6*, 307.
[45] H. Kawanishi, K. Ishizumi, I. Takahashi, H. Terauchi, Y. Hayafuji, *Jpn. J. Appl. Phys.* **2006**, *46*, 1067.
[46] J. Ravez, *C. R. Acad. Sci., Ser. IIC: Chem.* **2000**, *3*, 267.
[47] W. Warren, J. Robertson, D. Dimos, B. A. Tuttle, G. E. Pike, D. A. Payne, *Phys. Rev. B: Condens. Matter* **1996**, *53*, 3080.
[48] M. Ahart, M. Somayazulu, R. E. Cohen, P. Ganesh, P. Dera, H.-K. Mao, R. J. Hemley, Y. Ren, P. Liermann, Z. Wu, *Nature* **2008**, *451*, 545.
[49] P. Garcia-Fernandez, J. A. Aramburu, M. T. Barriuso, M. Moreno, *J. Phys. Chem. Lett.* **2010**, *1*, 647.
[50] P. S. Halasyamani, *Chem. Mater.* **2004**, *16*, 3586.
[51] E. A. Zhurova, V. G. Tsirelson, *Acta Crystallogr. B* **2002**, *B58*, 567.
[52] M. Zeng, S. W. Or, H. L. W. Chan, *J. Appl. Phys.* **2010**, *107*, 043513.
[53] M. Gröting, S. Hayn, K. Albe, *J. Solid State Chem.* **2011**, *184*, 2041.
[54] W. Krauss, D. Schütz, F. A. Mautner, A. Feteira, K. Reichmann, *J. Euro. Ceram. Soc.* **2010**, *30*, 1827.
[55] V. M. Goldschmidt, *Naturwissenschaften* **1926**, *14*, 477.
[56] W.-C. Lee, C.-Y. Huang, L.-K. Tsao, Y.-C. Wu, *J. Eur. Ceram. Soc.* **2009**, *29*, 1443.
[57] J. Kling, S. Hayn, L. A. Schmitt, M. Gröting, H.-J. Kleebe, K. Albe, *J. Appl. Phys.* **2010**, *107*, 114113.
[58] A. Slodczyk, P. Colomban, M. Pham-Thi, *J. Phys. Chem. Solids* **2008**, *69*, 2503.
[59] A. V. Turik, A. A. Yesis, L. A. Reznitchenko, *J. Phys.: Condens. Matter* **2006**, *18*, 4839.
[60] H. Uršič, M. Škarabot, M. Hrovat, J. Holc, M. Skalar, V. Bobnar, M. Kosec, I. Muševič, *J. Appl. Phys.* **2008**, *103*, 124101.
[61] J. Shi, H. Fan, Z. Li, *Ferroelectrics* **2011**, *404*, 93.
[62] X. Tan, J. C. Frederick, C. Ma, W. Jo, J. Rödel, *Phys. Rev. Lett.* **2011**, *105*, 2.
[63] D. Damjanovic, *IEEE Trans. Ultrason. Ferroelect. Freq. Control* **2009**, *56*, 1574.
[64] M. Hinterstein, M. Knapp, M. Hölzel, W. Jo, A. H. Cervellino, H. Ehrenberg, H. Fuess, *J. Appl. Crystallogr.* **2010**, *43*, 1314.
[65] L. Luisman, A. Feteira, A. K. Reichmann, *Appl. Phys. Lett.* **2011**, *99*, 192901.